Nanoscale

RSC Publishing

PAPER

Protein-encapsulated gold cluster aggregates: the case of lysozyme†

Cite this: *Nanoscale*, 2013, **5**, 2009

Ananya Baksi,[a] Paulrajpillai Lourdu Xavier,[a] Kamalesh Chaudhari,[ab] N. Goswami,[c] S. K. Pal[c] and T. Pradeep*[a]

Received 15th October 2012
Accepted 26th December 2012

DOI: 10.1039/c2nr33180b

www.rsc.org/nanoscale

We report the evolution and confinement of atomically precise and luminescent gold clusters in a small protein, lysozyme (Lyz) using detailed mass spectrometric (MS) and other spectroscopic investigations. A maximum of 12 Au^0 species could be bound to a single Lyz molecule irrespective of the molar ratio of Lyz : Au^{3+} used for cluster growth. The cluster-encapsulated protein also forms aggregates similar to the parent protein. Time dependent studies reveal the emergence of free protein and the redistribution of detached Au atoms, at specific Lyz to Au^{3+} molar ratios, as a function of incubation time, proposing inter-protein metal ion transfer. The results are in agreement with the studies of inter-protein metal transfer during cluster growth in similar systems. We believe that this study provides new insights into the growth of clusters in smaller proteins.

1 Introduction

One of the emerging categories of noble metal nanosystems is their ligand protected, atomically precise, quantum confined analogues, with a core size less than 2 nm. They are referred to as quantum clusters[1–4] (QCs) (also referred to as clusters, quantum confined/sized clusters, metal quantum dots, nanoclusters and superatoms). They exhibit intense luminescence besides distinct optical absorption features due to inter-band and intra-band transitions. Several monolayer protected clusters of this family have been investigated in detail[5–15] and in some cases, crystal structures are also known. For example, the total structures of monolayer protected gold clusters such as $Au_{25}(SR)_{18}$, Au_{38} $(SC_2H_4Ph)_{24}$, $Au_{102}(p\text{-MBA})_{44}$ and more recently, $Au_{36}(SPh\text{-}tBu)_{24}$ have been determined by X-ray crystallography.[13–17] A new window of opportunity has opened up with the creation of quantum clusters using macromolecular templates, where bigger molecules such as DNA,[18] dendrimers,[19,20] *etc.* have been used for cluster growth. New entrants to this fascinating family are protein-protected clusters.[1,21–35] Although they have well-defined molecular compositions and distinct luminescence characteristics, their optical absorption features are ill-defined in comparison to their ligand-protected analogues.[5–17] Both gold and silver clusters, protected with large proteins such as bovine serum albumin (BSA, 66.7 kDa),[21–25] lactotransferrin (Lf, 83.3 kDa),[26,27] and small proteins such as lysozyme (Lyz, 14.3 kDa),[28–32] insulin,[33] (5.8 kDa) horse radish peroxidase[34] and pepsin,[35] have been reported. Recently, AuAg alloy clusters have been synthesized in BSA.[25] Inter-cluster interaction between such clusters produces alloy systems whose compositions are tunable.[25] The luminescence of these protein-protected clusters has been used for biolabeling.[1,22,33,36,37] While functional proteins are fragile in general, a few reports indicating the retention of chemical reactivity and protein's bio-activity are available, however whether this robustness is applicable to many other cluster forming proteins is yet to be known.[33]

Myriad efforts have been made to understand the biomineralization process in the recent past, especially, biomineralization by proteins. Wei *et al.*[31] designed an experiment in which they grew plasmonic nanoparticles inside single lysozyme crystals. They could identify gold (in the ionic form)-bound amino acids by determining crystal structures as a function of time. MS has been the most suitable method to characterize metal clusters, though X-ray crystallography is ideal. We attempted to understand the growth of Au_{QCs} in Lf by time-dependent MS.[27] In these systems, evolution of the cluster core occurs gradually through an Au^{1+} intermediate in solution. Lf forms a thiolate-type of intermediate characterized by a well-defined Au^{1+} feature in the photoemission spectra.[27] Chemical reduction of this intermediate in alkaline pH gradually nucleates the Au cluster. Along with the cluster evolution, the protein is regenerated from the Au^{1+} complex. One of the important questions in such clusters is whether the cluster is generated inside the protein or it grows in-between a few protein molecules.

[a]*DST Unit of Nanoscience, Department of Chemistry, Indian Institute of Technology Madras, Chennai-600036, India. E-mail: pradeep@iitm.ac.in*

[b]*Department of Biotechnology, Indian Institute of Technology Madras, Chennai-600036, India*

[c]*Unit of Nanoscience and Technology, Department of Chemical, Biological and Macromolecular Sciences, Satyendra Nath Bose National Centre for Basic Sciences, Block JD, Sector III, Salt Lake, Kolkata 700 098, India*

† Electronic supplementary information (ESI) available. See DOI: 10.1039/c2nr33180b

A detailed investigation of the growth processes and distinction between these two possibilities require detailed mass spectrometric studies at different stages of growth. The reduction in instrumental resolution and ion transmission at large masses makes it difficult to explore the details of molecular changes in every system, especially in larger proteins. In the present study, instead of Lf or BSA, which are bulky in nature, we have chosen a small protein, Lyz, and probed how different it is from the larger protein analogues. It is important to emphasize that computations have shown that cluster growth within proteins is feasible. Large organic molecules such as dendrimers containing multiple thiol groups can completely wrap an Au_{55} cluster through gold–thiol interactions.[20] Ackerson and Sexton studied the binding of Au_{144} with neuro-proteins through thiol linkers and estimated the rigidity and positional displacement of the cluster using single particle cryo-electron microscopy.[38]

In this paper, we examine the growth of Au clusters in Lyz, a fairly small protein, which allows detailed examination by mass spectrometry. Lyz has a molecular weight of 14.3 kDa. It has 129 amino acid residues including 8 cysteines. These cysteine residues form 4 disulphide bonds located between the positions, 6–127, 30–115, 64–80 and 76–94. Unlike in proteins such as Lf, the mass spectrum of Lyz is characterized by intense features due to dimer, trimer and other higher oligomers. Previously, a few groups have used Lyz for gold cluster synthesis,[28–32] however, the size and growth of gold clusters synthesized in Lyz have not been ascertained through MS. Our study, presented in this paper, conclusively established that the cluster growth happens under the strong influence of cysteines. The chemistry of the cluster encapsulated protein seems to be similar to that of free protein as both of them form similar kinds of aggregates. In monolayer-protected clusters, multiple ligands bind to the cluster surface, while in the case of large proteins, a single molecule of protein acts as a wrapping entity. In the case of BSA or Lf, with high molecular weight, the large number of thiol groups (34 and 36 cysteine residues) and bulky nature may facilitate the formation of clusters within a single protein molecule.[21–27] The small protein used here is intermediate between small ligands and larger proteins with a relatively less number of available S–S groups.[28–33] This investigation will rationally establish the relationship between the protein (ligand) size and the cluster formed and also the number of stabilizing groups binding the cluster surface in encapsulated clusters of this kind. The associated properties of the clusters such as luminescence are discussed only to a limited extent as these aspects have been discussed earlier.[1,21–33]

2 Experimental

2.1 Reagents and materials

Tetrachloroauric acid trihydrate ($HAuCl_4 \cdot 3H_2O$) was prepared in our lab starting from elemental gold. Sodium hydroxide (Rankem, India) was purchased from the local supplier. Lysozyme (>90% purity) and sinapic acid (~99% purity) were purchased from Sigma-Aldrich. All the chemicals were used without further purification. Deionized water was used in all the experiments.

2.2 Instrumentation

For MALDI TOF MS analysis, an Applied Biosystems Voyager De Pro instrument was used with sinapic acid as the matrix. A pulsed nitrogen laser of 337 nm was used for ionizing the sample. Spectra were collected in the positive mode and an average of 250 shots was used for each spectrum. The matrix was prepared by dissolving 10 mg of sinapic acid in a 1 : 3 mixture of acetonitrile: 0.1% trifluoroacetic acid (overall volume of 1 mL). While preparing samples for analysis, 5 μL of the cluster solution, without dilution, was mixed thoroughly with 100 μL of the matrix mixture. 2.5 μL of the resulting mixture was used for spotting. For ESI MS analysis, 10 μL of the sample was taken and diluted to 2 mL with DI water. Trifluoroacetic acid (TFA) (0.1% in DI, 10 μL) was added as an ionization enhancer for spectral collection in the positive ion mode. A Thermo Scientific LTQ XL ESI MS instrument was used for this study. Ion spray voltage was kept at 4.5 kV and the capillary temperature was set at 250 °C. XPS analysis was done to confirm the reduction of Au^{3+} to Au^0. A powdered sample was spotted on the XPS plate. An Omicron ESCA probe spectrometer was used for XPS analysis. Polychromatic Mg Kα ($h\nu = 1236.6$ eV) was used as the ionization source. Curves were smoothed and fitted using the CasaXPS software. Luminescence measurement was carried out in a Jobin Yvon NanoLog fluorescence spectrometer with a band pass of 3 nm for both emission and excitation spectra. UV/Vis spectra were collected using a PerkinElmer Lambda 25 spectrometer in the range of 200–1100 nm. Scanning Electron Microscopic (SEM) and Energy Dispersive Analysis of X-rays (EDAX) images were collected using an FEI QUANTA-200 SEM instrument. High Resolution Transmission Electron microscopic (HRTEM) images were taken using a JEOL 3010 instrument. Picosecond-resolved fluorescence decay transients were measured using a commercially available spectrophotometer (Life Spec-ps, Edinburgh Instruments, UK) with 60 ps instrument response function (IRF). The observed luminescence transients were fitted with a nonlinear least square fitting procedure to a function $(X(t)) = \int_0^t E(t')R((t-t')\mathrm{d}t')$ comprising convolution of the IRF ($E(t)$) with a sum of exponential $\left(R(t) = A + \sum_{i=1}^{N} B_i e^{-t/\tau_i}\right)$ with pre-exponential factors (B_i), characteristic lifetimes (τ_i) and a background (A). Relative concentration in a multi-exponential decay was finally expressed as: $c_n = \frac{B_n}{\sum_{i=1}^{N} B_i} \times 100$. The quality of the curve fitting was evaluated by reduced chi-square. It has to be noted that with our time resolved instrument, we can resolve at least one fourth of the instrument response time constants after de-convolution of the IRF. The Circular Dichroism (CD) spectra were measured in a Jasco 815 spectropolarimeter with a Peltier setup for the temperature-dependent measurements. CD studies were done with a 10 mm path length cell.

2.3 α-Helix calculation

Alpha helix content was calculated from the obtained CD spectra by the formula proposed by Chen *et al.*[39] (α-helix

(%) = $-(\theta + 3000)/39\,000$, where $\theta = \text{MRW} \times \theta_{222}/10lc$, where MRW is mean residual weight (110.9 g per residue for Lyz), θ_{222} is the angle at the wavelength 222 nm, l is path length of the cell (1 cm) and c is the concentration of the sample used for the measurement (10^{-7} g mL^{-1})).

2.4 Synthesis

The synthetic approach for creating luminescent gold clusters was similar to the previously employed methods.[21] Briefly, it involves incubating Lyz with Au^{3+} at a molar ratio of 1 : 4 for 12 hours. The final concentration was 150 μM and 0.625 mM for Lyz and Au^{3+}, respectively. The pH was adjusted to 12 using 1 N NaOH, after adding Au^{3+}. Appearance of red luminescence after 4 hours indicated the formation of clusters in solution. Time and concentration-dependent experiments were conducted for better understanding of the cluster growth mechanism. Most of these were carried out in the solution phase using the as-prepared clusters directly. Several protein-to-gold ratios (1 : 2.5, 1 : 4, 1 : 5, and 1 : 8) were used.

3 Results and discussion

3.1 Formation of Au_{QC}@Lyz and its characterization

Parent Lyz shows its well-defined molecular feature at m/z 14 300 in the linear positive ion MALDI MS spectrum. It is also characterized by the presence of different molecular aggregates at m/z 28 800, 42 900, 57 200 corresponding to dimer, trimer and tetramer, respectively, with a gradual decrease in intensity (blue trace, Fig. 1). Such aggregation can happen in the solution phase as well due to salt bridges formed between the proteins.[40] In the lower mass region ($<m/z$ 8000), the spectra are dominated by multiply charged species and a few fragments. In Fig. 1 (red trace) the spectrum corresponds to the reaction product of 1 : 4 molar ratio of Lyz : Au at pH 12. A unique feature due to the metal cluster appears at m/z 16 270, shifted by m/z 1970 from the parent Lyz, due to 10 Au atoms. This peak is attributed to a quantum cluster of Au_{10} core formed within the protein, referred to as Au_{QC}@Lyz. The di-, tri-, tetra- and even pentamer of Au_{QC}@Lyz showed similar patterns of bound Au atoms. The total number of Au atoms bound, divided by the number of protein molecules in the aggregate confirmed the distribution of 10 Au atoms per protein in each case. This suggests that each protein entity contains a strongly bound, ten-atom gold nanostructure. Further, it signifies that the observed di-, tri-, tetra-, and pentamers are likely to be aggregates of individual protein molecules, each containing a ten-atom cluster of gold within, rather than aggregates of protein molecules bound to a multi-atom gold species. In the latter case, the number of Au atoms cannot increase systematically in multiples of 10 with the aggregation number. Interestingly, it was the cluster feature which was more prominent in the entire mass range and beyond the trimer region; free protein features were nearly absent. The monomer region expanded in the inset of Fig. 1 shows distinct binding of Au to the parent protein. The mass spectrum of Au_{QC}@Lyz exhibits an increased width after the attachment of gold (inset of Fig. 1). This is evident in the monomer region of the parent protein which also shows distinct features spaced by m/z = 197 due to Au ion uptake. The cluster features were stable although minor changes in the nuclearity of the cluster core is evident with time in the monomer region (Fig. S1†). However, the trimer, tetramer and

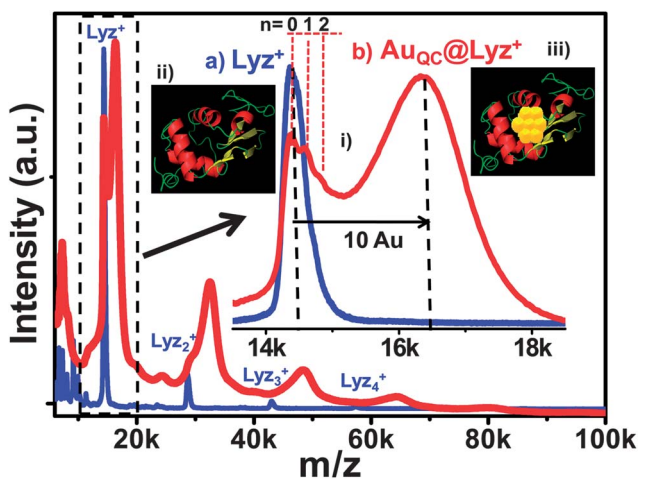

Fig. 1 Positive ion MALDI MS of Lyz at pH 12 in linear mode (a) and Au_{QC}@Lyz after 24 hours of incubation (b). All the spectra were measured in the linear positive mode over the m/z range of 2000–100 000. Both Lyz and Au_{QC}@Lyz showed aggregate formation. The expanded monomer region in inset (i) clearly shows a separation of 10 Au atoms from the parent protein. In the dimer, trimer, tetramer and pentamer regions, the separations are of 20, 30, 40 and 50 Au atoms, respectively. In insets (ii) and (iii), schematic representations of Lyz and Au_{QC}@Lyz, respectively, are shown.

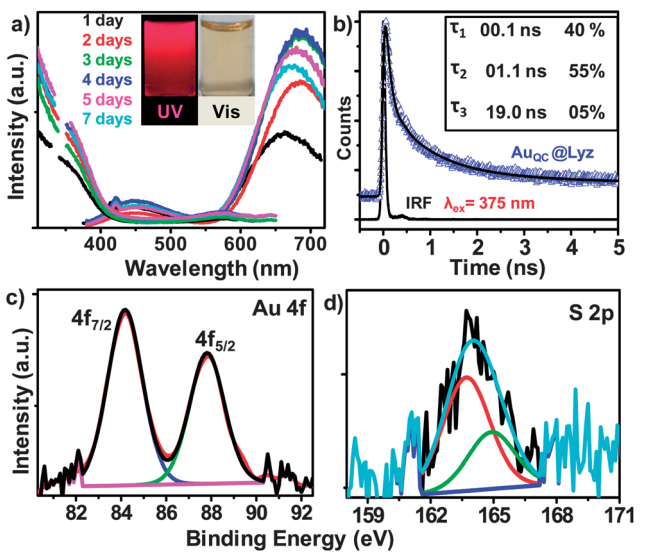

Fig. 2 (a) Time dependent luminescence spectra of the as-synthesized Au_{QC}@Lyz at 365 nm excitation showing an emission maximum around 680 nm. The inset photographs show the color of the cluster solution under ultraviolet and visible radiations, respectively. (b) Luminescence decay of Au_{QC}@Lyz with instrument response function (IRF) ~80 ps. Lifetime values are shown in the inset. Standard error of time components is ~10%. X-ray photoelectron spectra of the as-synthesized Au_{QC}@Lyz showing the presence of (c) Au^0 in Au 4f and (d) thiolate BE in S 2p.

other oligomers did not show significant change over the period investigated. This change in nuclearity is also reflected in the luminescence profile which shows a shift of nearly 25 nm in this time window (Fig. 2a). Two emission maxima, one at 450 nm (which is likely to be from the protein alone, and it has been observed in several instances involving metal ion reduction by aromatic amino acids[26,27,41,42] and also upon the oxidation of protein's intrinsic fluorophores[43]) and the other at 686 nm were observed and the latter was blueshifted to 661 nm after 5 days (excitation wavelength was 365 nm) while the former remained the same. As there is a slight change in the core size, the luminescence is also blueshifted (see the MS data (Fig. S1†)). The decrease in mass spectral intensity of the cluster is evident in the luminescence spectrum as well. Up to a certain period of time, the intensity goes on increasing and after that it again starts decreasing along with a slight blueshift in the peak position. This shift may be due to the loss of one Au atom from the core which is evident from the mass spectral analysis. As luminescence in protein encapsulated noble metal clusters has been studied earlier[21–36] we presented only the essential aspects of relevance here.

The calculated quantum yield (QY) of the cluster is nearly 15.6% taking Rhodamine 6G as the standard (QY = 95% at 488 nm excitation in water).[23] The luminescence decay of the Au_{QC}@Lyz in water was measured by a picosecond-resolved time-correlated single-photon counting (TCSPC) technique. Fig. 2b demonstrates the decay transients of the Au_{QC}@Lyz. Lifetime values of the clusters were obtained by numerical fitting of the luminescence at 650 nm. Lifetimes of Au_{QC}@Lyz were 0.1 ns (40%), 1.1 ns (55%) and 19.0 ns (5%) (see Fig. 2b). Similarity of the lifetime components with the reported other protein protected clusters reveals that the 650 nm emission is coming predominantly from the Au QCs. The obtained lifetime values, in comparison with the previous reports of Au_{25}@proteins,[22,26] suggest this species to be smaller than Au_{25} and the reduction in lifetime is distinct in the short and long components, which in turn is supported by the MS data.

Fluorescence in ligand-protected Au_{QCs} is largely influenced by the nature of the ligands and is not fully understood yet. Murray and co-workers[44] showed that in the case of Au_{38} and Au_{140}, the near infrared luminescence intensity increased linearly with the proportion of polar thiolate ligands. Although there were insignificant changes in the absorption spectra of various ligand exchanged Au_{25} clusters, noticeable changes were seen in their luminescence spectra.[45] Jin and Wu[46] also have recently shown that ligands and their length play a vital role in the luminescence of Au_{25}. Recently, in thiolate protected AuAg alloy clusters, an increase in fluorescence lifetime was observed as a function of ligand length.[47] These observations propose that in bulky ligands as in proteins, there are several contributing effects which enhance the luminescence intensity. Factors such as multiple interaction sites facilitating electron and energy transfer between the amino acids, isolation of the metal core from the medium as seen in Au_{15}@cylcodextrin[48] and distinct Förster resonance energy transfer (FRET) are expected to play crucial roles in the observed high luminescence. We note, however, that the electronic structure of protein encapsulated clusters is entirely different from their monolayer protected analogues as manifested in the differences in their absorption spectra.

Existence of a nearly metallic (Au^0) cluster core is further supported by the photoemission data. Au $4f_{7/2}$ appears at 84.2 eV close to the Au^0 binding energy (BE) (Fig. 2c). The BE is slightly higher than the same for Au^0 due to the core size effect and the bonding environment. $4f_{7/2}$ binding energy values for Au^{3+}, Au^{1+} and Au^0 are 87.3, 85.4 and 84.0 eV, respectively.[25,27] S 2p BE confirms the presence of Au–S bonding (Fig. 2d). The S $2p_{3/2}$ occurs at 163.0 eV which supports the thiolate binding on the Au core. The Au : S atomic ratio found was 12 : 7, which is close to the value corresponding to 10 Au and 8 S, per cluster. Also, it reveals the absence of excess sulphur, unlike that observed in clusters formed with larger proteins like BSA or Lf.[25,26] The spectral width is slightly higher than that observed for Au thin films, suggesting the possibility of multiple oxidation states present in the clusters. No other component such as sulphate, or sulphonate was observed. This may be attributed to the absence of X-ray-induced damage in the sample which supports the complete protection of the cluster core. From the survey spectrum (shown in Fig. S2†) we confirm the existence of all the possible elements: carbon, nitrogen, oxygen, sodium, chlorine, gold and sulphur. All the BE values are corrected with respect to the C 1s binding energy of 285.0 eV. Energy dispersive analysis of X-rays (EDAX) also confirmed the presence of all the elements (Fig. S3†).

A HRTEM study revealed that these clusters have a core size of 1.1 ± 0.1 nm, which is in good agreement with the size of protein protected noble metal clusters (inset of Fig. S4†). Although it is not a confirmative tool to know the size of protein-protected clusters, the observation conclusively establishes the absence of bigger nanoparticles in solution. The common spectroscopic tool, UV/Vis, is inadequate to identify the nature of the core in protein protected gold nanoclusters, since they do not exhibit well defined features of the core unlike the monolayer protected analogues which have well-defined spectroscopic features and are sensitive even in a minor change in the core size. The UV/Vis spectra show two peaks: one near 290 nm which is a characteristic of aromatic amino acids in proteins and the other (hump) around 353 nm, possibly due to oxidized aromatic amino acid residues[42] (Fig. S4†). No plasmon resonance peak was observed which again confirms the absence of bigger nanoparticles in solution.

3.2 Difference in alkali metal binding and Au binding

Binding of metal ions to proteins is expected. However, binding with noble metals is distinctly different in comparison to common ions such as alkali metals. To see this difference, we have performed electrospray ionization mass spectrometry (ESI MS) studies. In the control experiment, 0.1 mM alkali metal chlorides were added to Lyz and ESI MS was recorded (Fig. 3a). The spectra are expanded in the +8 charge state region, in the inset. As the size of the metal ion increases from Na to Cs, the number of attachments decreases. For Na and K, addition of up to 5 metal ions is seen at that concentration; but for Rb it is up

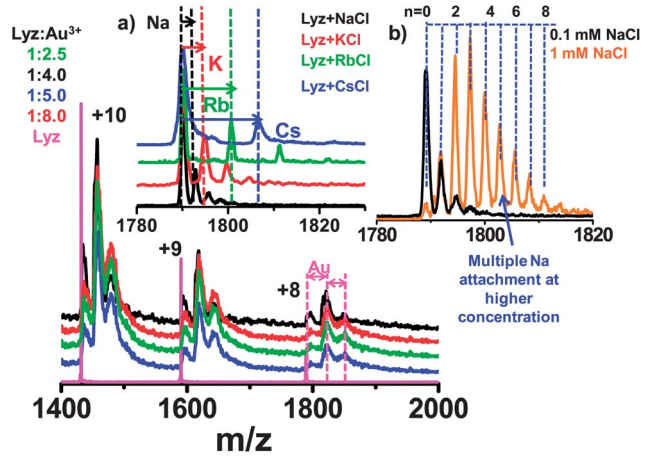

Fig. 3 ESI MS of the Lyz and Au^{3+} mixture without the addition of base showing a fixed number of Au atom attachments to Lyz irrespective of the concentration used. A maximum of three Au atoms are attached to Lyz at the experimental condition. Inset (a) shows different metal ion uptakes at a very low concentration of metal chlorides. Separations from the main protein peak are due to different metal ion uptakes. While Na and K ions show multiple uptakes due to a smaller size, Rb and Cs ions show a limited number of uptakes at the same condition. In inset (b), multiple Na atom attachments are seen at a higher concentration of NaCl, revealing that binding sites for alkali metal atoms are different from that for Au atoms.

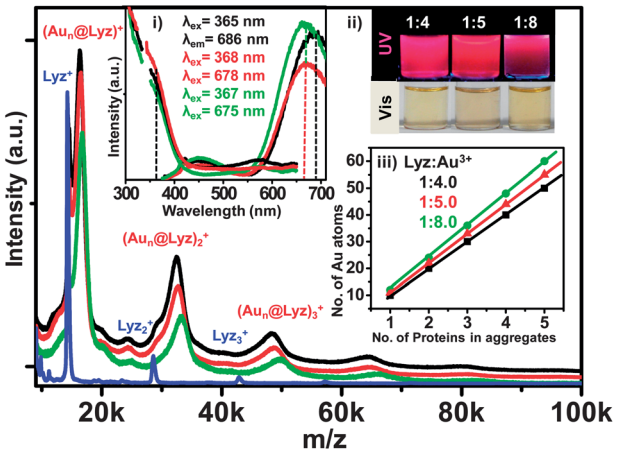

Fig. 4 Concentration dependent MALDI MS at various Lyz to Au^{3+} molar ratios: 1 : 2.5, 1 : 4, 1 : 5 and 1 : 8. Numbers of Au atoms in the cores are 10, 11 and 12 for Lyz to Au^{3+} ratios of 1 : 4, 1 : 5 and 1 : 8, respectively. Inset (i) shows comparative luminescence spectra of different concentrations of Au^{3+}. The excitation wavelengths do not change significantly for different Lyz to Au^{3+} ratios. Emission peak positions vary from 675 to 686 nm (for time dependent luminescence spectra see Fig. 2 and S8–S10†). Inset (ii) shows photographs of different cluster solutions under ultra-violet and visible light. In inset (iii) a comparative plot of the number of gold ions uptaken by various oligomers at different protein to Au^{3+} concentrations after 7 days is shown. Au uptake by different oligomers shows a linear dependence.

to 3 and for Cs it is only up to 2. The same experiment was carried out using a high concentration (1 mM) of Na^+. In this condition, nearly 10 Na ions were bound to the protein (Fig. 3b). So it can be concluded that the number of Na ion uptake increases with increasing concentration. Various mixtures of Lyz : Au^{3+} ratios were taken; namely, 1 : 2.5, 1 : 4, 1 : 5 and 1 : 8. In the ESI MS for all cases (Fig. 3), the same number of Au atom attachments was seen. Au atoms are likely to bind to the cysteine residues of the protein. In Lyz, there are 8 cysteine units to bind with Au, although we see only a few attachments. This may be due to the high charge state of the protein which cannot stabilize large number of Au atoms and overlapping of one charge state region with the next one does not allow us to resolve the exact number of Au atom attachments. On the other hand, there are several carboxyl and hydroxyl groups in the protein for the uptake of alkali metal ions. If we keep on increasing alkali metal ion concentration, proteins will show uptake until all the sites are occupied. But there are also a limited number of free carboxyl and hydroxyl groups; hence alkali metal ion attachment cannot go beyond this. From this study, it is evident that binding of Au is totally different from binding in alkali metal ions. While Au binding is strongly influenced by cysteine residues, alkali metals prefer to bind with the carboxyl and hydroxyl groups of different amino acid residues.

3.3 Dependence of Au^{3+} concentration: clusters and cluster dimers, trimers, mixed dimers

While cluster binding to the protein is evident in Fig. 1 and 4, it is not conclusive whether the cluster is encapsulated within it or not. One of the definite proofs for the existence of the cluster core within is the systematic shift observed in the mass of the protein aggregates. We explored this in two different cases, high and low exposures of gold. The higher concentration regime is discussed first. The amount of Au ion uptake is weakly sensitive to the quantity of Au exposed. Average cluster size ranges from 10–12 in protein to metal ratios of 1 : 4, 1 : 5 and 1 : 8 (Fig. 4). Such cores are designated as Au_{10-12} in the text below. Uptake in the dimer and oligomer regions is directly proportional to the uptake shown by the monomer. At no region of the mass spectrum is seen a trimer or tetramer with the same core as seen in the monomer (Fig. S5 and S6†). The absence of $Au_{10-12}@(Lyz)_{2,3,...}$ species suggests the absence of entities where a single Au_{10-12} core is surrounded by several protein molecules in solution. This is also supported by the metal ion uptake by the parent protein, which shows a series of Au uptake peaks. In the dimer region, a feature appears where the separation between the parent dimer and the new feature is double that of the corresponding peaks in the monomer region. This would imply that the formation of aggregates is either a solution phase effect and are not formed in the gas phase due to the association reactions between vapor phase species. In association reactions, there are multiple possibilities which are not observed. This kind of shift is seen in higher aggregates such as thrice in trimer, quadruple in tetramer, *etc.* This systematic change is depicted in Fig. 4iii. In the lowest concentrations alone, some non-uniformity is seen as mentioned above which appears to be due to the presence of excess protein in which most of the binding sites for gold are free. Although these aggregates exist in the solution, the photophysical properties of the clusters do not show their presence. This appears to be due to large inter-cluster distance as each cluster core is surrounded

by a protein shell. Taking the overall size of Lyz to be nearly 4 nm, the inter-cluster distance is 8 nm which is much larger than that which would facilitate electronic interaction between the cores. This is manifested in the luminescence spectra where only very minor shifts are seen (Fig. 4i). No observable effect is seen in the photographs (Fig. 4ii).

3.4 Cluster growth mechanism: multiple cluster growth through the regeneration of free protein

This change is even more dramatic in the time dependent case presented in Fig. 5 at low concentration, upon exposure of Au over a long time. It is the lowest protein to Au^{3+} conc. ratio that was examined. At a shorter incubation time, of the order of a day, a shoulder comes at a separation of 10 gold atoms in the monomer region while the shift was neither 10 nor 20 in the dimer region. It is a broad hump in-between 10 and 20 Au atoms. With time (for time dependent study see Fig. S7†), the peak in the monomer region starts shifting to a higher mass of 12 Au atoms separation and interestingly the dimer region gets divided into two peaks; one due to 12 Au atoms and another due to ~20 Au atoms. The same thing happens to the trimer region also where peaks are separated by ~12 and ~22 Au atoms. For the tetramer, the separations are 12 and 26 Au atoms. Because of the broad hump, it was not possible to identify other species in the trimer and tetramer regions. After the tetramer region, it is hard to resolve the peak separation due to reduced intensity. As explained earlier, there is a gradual emergence of free protein with time in the cluster system. These free proteins enable the formation of Au_{10-12}@Lyz–Lyz along with $(Au_{10-12}$–$Lyz)_2$ and the possibility of the former increases with time as free Lyz concentration increases. As a result, the dimer region exhibits both these features (Au_{10-12}@Lyz–Lyz and $(Au_{10-12}$–$Lyz)_2$) with a characteristic mass shift. As the free Lyz concentration keeps increasing with time, the dimer region shows only Lyz_2 and Au_{10-12}@Lyz–Lyz features. Corresponding changes are seen in the larger aggregates as well. It is important to note that if one cluster is surrounded by multiple proteins, we would have observed Au_{10-12}–Lyz_n features prominently for dimer, trimer, *etc.* and these are not seen. Instead $(Au_{10-12}$@$Lyz)_n$ features are dominant.

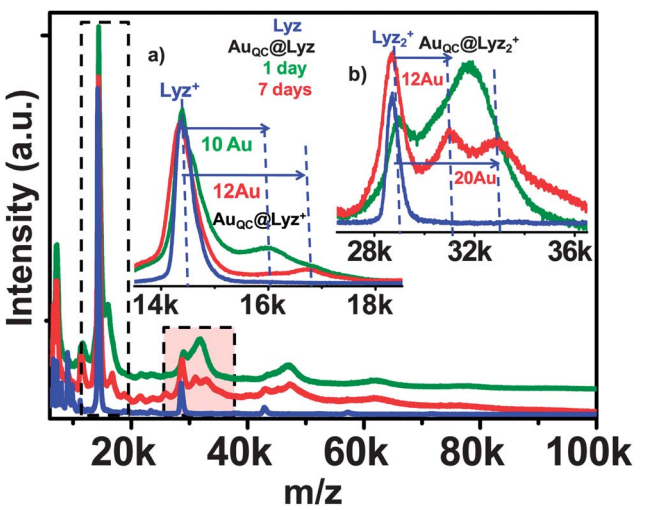

Fig. 5 MALDI MS of a Au_{QC}@Lyz, where the lowest Lyz to Au^{3+} molar ratio (1 : 2.5) was used. There is a clear change in the spectra as the storage time changes from one day (green trace) to 7 days (orange trace). Insets: (a) expanded view of the monomer region and the (b) dimer region. The trimer also has two different separations at 12 and 22 Au atoms. For higher oligomers, the separation was not resolvable.

3.5 Change in the protein secondary structure

Formation of the cluster affects the secondary structure of the protein. Large changes were seen in the fraction of α helices after cluster formation, as a loss of 28% (total helix content decreased from 49% to 21%) was observed in the circular dichroism (CD) spectra. This may be correlated to the structure of lysozyme where cysteine residues are present (at 6, 30, 64, 80, 115 and 127 amino acid positions)[49] and four of which are located in the vicinity of α helices.[41] As the disulphides were broken and used to stabilize the cluster core, drastic changes in the total helix content was observed. Computational studies showed that the disulphide bond can break upon the addition of Au^{3+} to Lyz, as one disulphide bond breaks to give two sulphur ends and two electrons are donated to form the cluster core upon the addition of Au^{3+} alone.[50] A net loss of α-helix structure and increase in β-sheets and random coils is evident from the FTIR spectra, as follows, corroborating the CD observations.

Distinct changes in the amide region were observed. Amide bands I, II and III are characteristic of the protein's secondary structure.[26,51] The band near 1650 cm^{-1} arises mainly from the C=O stretching vibration with a minor contribution from the out of plane C–N stretching. This is attributed as the amide I signature. Another band near 1550 cm^{-1} is due to the out of phase combination of NH in plane bending with a smaller contribution from C=O in plane bending as well as C–C, and C–N stretching. The region 1400–1200 cm^{-1} is due to amide III vibrational modes. A significantly broad band arises near 3300–3000 cm^{-1} due to N–H and O–H stretching vibrations. This region is ascribed as a mixture of amide A and amide B.[26,51] From the IR data (Fig. S11†), it is clear that there are changes in

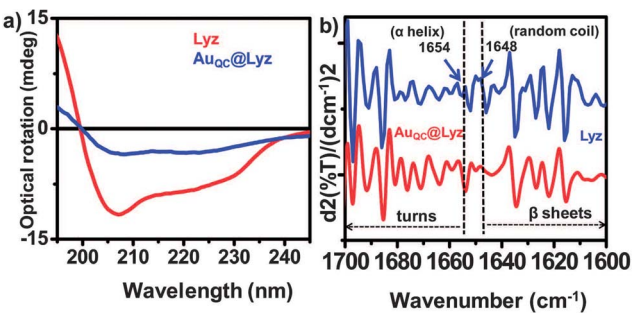

Fig. 6 (a) CD spectra of Lyz and as prepared Au_{QC}@Lyz showing a clear change in ellipticity of the spectra, which indicates a huge change in the alpha helical structure. (b) Double derivative of the infrared (IR) spectra shows the disappearance of the peak at 1654 cm^{-1} in the case of Au_{QC}@Lyz.

the amide region. A band near 700 cm^{-1} can be attributed to $-NH_2$ and NH wagging. Bands at values >2950 cm^{-1} are due to C–H stretching in $-CH_3$, $-CH_2$, and –CH groups. The O–H stretching frequency is also observable as a broad peak around 3500 cm^{-1}. Second derivative IR (in the region 1600–1700 cm^{-1}), which is more sensitive, revealed the changes in the amide region due to cluster formation. Among α-helix (1651–1658 cm^{-1}), β-sheets (1618–1642 cm^{-1}), random coils (1640–1650 cm^{-1}) and turns (1666–1688 cm^{-1}), the α-helix region showed large changes. A clear change can be seen in the α-helix feature at 1654 cm^{-1} which is completely absent in the case of the cluster, because of the huge perturbation of the α-helical regions, which may be due to breakage of disulphide bonds for cluster formation as mentioned above (Fig. 6).

4 Summary and conclusion

A mass spectrometric investigation to understand the nature of gold cluster formation by small proteins, represented by the model protein, lysozyme has been performed. The red emitting cluster formed is of ~10 Au atoms, which is smaller than the reported cluster size in bigger proteins such as BSA or Lf. An interesting phenomenon of protein aggregates formed by cluster containing proteins was observed. Furthermore, the emergence of free protein during the synthesis suggested interprotein metal transfer. In conclusion, we suggest that small protein molecules, such as Lyz, can wrap and stabilize very small cluster cores consisting of 10, 11 and 12 Au atoms. The growth mechanism is highly dependent on the disulphide bond breakage where cysteine residues can form Au–S bonds and the core is stabilized by thiolate linkages. From a comparative study with alkali metal ions, we demonstrated the difference between the binding of Au and Na ions with the protein. Whereas Na^+ binds to carboxyl and hydroxyl groups, Au^+ prefers the sulphurs of cysteines for binding. An extensive MALDI MS study in the entire mass range of the protein and its aggregates suggests that the cluster is held within the protein molecule. In a nutshell, we have demonstrated a confirmative mass spectrometric analysis to prove endoprotein cluster growth using a small protein, Lyz, as a model. This is one of the first steps in understanding of the system and more steps are ahead to elucidate the exact mechanism of this kind of cluster growth. We believe that this study would rationally establish the relationship between the protein (ligand) size and the cluster formed. A detailed understanding of the protein conformational change and, probably, computer simulation of cluster growth would lead to new directions in this area.

Acknowledgements

We thank Department of Science and Technology for funding our research program on nanomaterials. A.B. and N.G. thank Council of Scientific and Industrial Research (CSIR) for a research fellowship. A.B. thanks Amitava Srimany, M. S. Bhootaraju and Jyoti Sarita Mohanty for useful discussions.

References

1 P. L. Xavier, K. Chaudhari, A. Baksi and T. Pradeep, *Nano Rev.*, 2012, **3**, 14767, and the references cited therein.
2 J. Zheng, P. R. Nicovich and R. M. Dickson, *Annu. Rev. Phys. Chem.*, 2007, **58**, 407–431.
3 J. Zheng, C. W. Zhang and R. M. Dickson, *Phys. Rev. Lett.*, 2004, **93**, 077402/1–4.
4 R. Jin, *Nanoscale*, 2010, **2**, 343–362.
5 T. U. B. Rao, B. Nataraju and T. Pradeep, *J. Am. Chem. Soc.*, 2010, **132**, 16304–16307.
6 M. Zhu, E. Lanni, N. Garg, M. E. Bier and R. Jin, *J. Am. Chem. Soc.*, 2008, **130**, 1138–1139.
7 Y. Negishi, K. Nobusada and T. Tsukuda, *J. Am. Chem. Soc.*, 2005, **127**, 5261–5270.
8 Y. Shichibu, Y. Negishi, T. Tsukuda and T. Teranishi, *J. Am. Chem. Soc.*, 2005, **127**, 13464–13465.
9 C. Kumara and A. Dass, *Nanoscale*, 2011, **3**, 3064–3067.
10 C. Kumara and A. Dass, *Nanoscale*, 2012, **4**, 4084–4086.
11 K. Kimura, N. Sugimoto, S. Sato, H. Yao, Y. Negishi and T. Tsukuda, *J. Phys. Chem. C*, 2009, **113**, 14076–14082.
12 M. W. Heaven, A. Dass, P. S. White, K. M. Holt and R. W. Murray, *J. Am. Chem. Soc.*, 2008, **130**, 3754–3755.
13 M. W. Heaven, A. Dass, P. S. White, K. M. Holt and R. W. Murray, *J. Am. Chem. Soc.*, 2008, **130**, 3754–3755.
14 M. Zhu, C. M. Aikens, F. J. Hollander, G. C. Schatz and R. Jin, *J. Am. Chem. Soc.*, 2008, **130**, 5883–5885.
15 H. Qian, W. T. Eckenhoff, Y. Zhu, T. Pintauer and R. Jin, *J. Am. Chem. Soc.*, 2010, **132**, 8280–8281.
16 P. D. Jadzinsky, G. Calero, C. J. Ackerson, D. A. Bushnell and R. D. Kornberg, *Science*, 2007, **318**, 430–433.
17 C. Zeng, H. Qian, T. Li, G. Li, N. L. Rosi, B. Yoon, R. N. Barnett, R. L. Whetten, U. Landman and R. Jin, *Angew. Chem., Int. Ed.*, 2012, **51**, 13114–13118.
18 J. T. Petty, J. Zheng, N. V. Hud and R. M. Dickson, *J. Am. Chem. Soc.*, 2004, **126**, 5207–5212.
19 X. Sun, X. Jiang, S. Dong and E. Wang, *Macromol. Rapid Commun.*, 2003, **24**, 1024–1028.
20 D. Thompson, J. P. Hermes, A. J. Quinn and M. Mayor, *ACS Nano*, 2012, **6**, 3007–3017.
21 J. Xie, Y. Zheng and J. Y. Ying, *J. Am. Chem. Soc.*, 2009, **131**, 888–889.
22 M. A. H. Muhammed, P. K. Verma, S. K. Pal, A. Retnakumari, M. Koyakutty, S. Nair and T. Pradeep, *Chem.–Eur. J.*, 2010, **16**, 10103–10112.
23 X. Le Guével, B. Hötzer, G. Jung, K. Hollemeyer, V. Trouillet and M. Schneider, *J. Phys. Chem. C*, 2011, **115**, 10955–10963.
24 A. Mathew, P. R. Sajanlal and T. Pradeep, *J. Mater. Chem.*, 2011, **21**, 11205–11212.
25 J. S. Mohanty, P. L. Xavier, K. Chaudhari, M. S. Bootharaju, N. Goswami, S. K. Pal and T. Pradeep, *Nanoscale*, 2012, **4**, 4255–4262.
26 P. L. Xavier, K. Chaudhari, P. K. Verma, S. K. Pal and T. Pradeep, *Nanoscale*, 2010, **2**, 2769–2776.
27 K. Chaudhari, P. L. Xavier and T. Pradeep, *ACS Nano*, 2011, **5**, 8816–8827.

28 H. Wei, Z. Wang, L. Yang, S. Tian, C. Hou and Y. Lu, *Analyst*, 2010, **135**, 1406–1410.
29 Y.-H. Lin and W.-L. Tseng, *Anal. Chem.*, 2010, **82**, 9194–9200.
30 W.-Y. Chen, J.-Y. Lin, W.-J. Chen, L. Luo, E. W.-G. Diau and Y.-C. Chen, *Nanomedicine*, 2010, **5**, 755–764.
31 H. Wei, Z. Wang, J. Zhang, S. House, Y.-G. Gao, L. Yang, H. Robinson, L. H. Tan, H. Xing, C. Hou, I. M. Robertson, J.-M. Zuo and Y. Lu, *Nat. Nanotechnol.*, 2011, **6**, 93–97.
32 T.-H. Chen and W.-L. Tseng, *Small*, 2012, **8**, 1912–1919.
33 C.-L. Liu, H.-T. Wu, Y.-H. Hsiao, C.-W. Lai, C.-W. Shih, Y.-K. Peng, K.-C. Tang, H.-W. Chang, Y.-C. Chien, J.-K. Hsiao, J.-T. Cheng and P.-T. Chou, *Angew. Chem., Int. Ed.*, 2011, **50**, 7056.
34 H. Kawasaki, K. Hamaguchi, I. Osaka and R. Arakawa, *Adv. Funct. Mater.*, 2011, **21**, 3508–3515.
35 F. Wen, Y. Dong, L. Feng, S. Wang, S. Zhang and X. Zhang, *Anal. Chem.*, 2011, **83**, 1193–1196.
36 M. A. H. Muhammed, P. K. Verma, S. K. Pal, R. C. A. Kumar, S. Paul, R. V. Omkumar and T. Pradeep, *Chem.–Eur. J.*, 2009, **15**, 10110–10120.
37 C.-A. J. Lin, T.-Y. Yang, C.-H. Lee, S. H. Huang, R. A. Sperling, M. Zanella, J. K. Li, J.-L. Shen, H.-H. Wang, H.-I. Yeh, W. J. Parak and W. H. Chang, *ACS Nano*, 2009, **3**, 395–401.
38 J. Z. Sexton and C. J. Ackerson, *J. Phys. Chem. C*, 2010, **114**, 16037–16042.
39 Y. H. Chen, J. T. Yang and K. H. Chau, *Biochemistry*, 1974, **13**, 3350–3359.
40 B. A. Persson, M. Lund, J. Forsman, D. E. W. Chatterton and T. Ãkesson, *Biophys. Chem.*, 2010, **151**, 187–189.
41 O. L. Muskens, M. W. England, L. Danos, M. Li and S. Mann, *Adv. Funct. Mater.*, 2013, **23**, 281–290.
42 S. Si and T. K. Mandal, *Chem.–Eur. J.*, 2007, **13**, 3160–3168.
43 N. Goswami, A. Makhal and S. K. Pal, *J. Phys. Chem. B*, 2010, **52**, 15236–15243.
44 G. Wang, R. Guo, G. Kalyuzhny, J.-P. Choi and R. W. Murray, *J. Phys. Chem. B*, 2006, **110**, 20282–20289.
45 E. S. Shibu, M. A. Habeeb Muhammed, T. Tsukuda and T. Pradeep, *J. Phys. Chem. C*, 2008, **112**, 12168–12176.
46 Z. Wu and R. Jin, *Nano Lett.*, **10**, 2568–2573.
47 T. Udayabhaskararao, Y. Sun, N. Goswami, S. K. Pal, K. Balasubramanian and T. Pradeep, *Angew. Chem., Int. Ed.*, 2012, **51**, 2155–2159.
48 E. S. Shibu and T. Pradeep, *Chem. Mater.*, 2011, **23**, 989–999.
49 R. Diamond, D. C. Phillips, C. C. F. Blake and A. C. T. North, *J. Mol. Biol.*, 1974, **82**, 371–391.
50 A. Baksi, T. Pradeep, B. Yoon, C. Yannouleas and U. Landman, submitted.
51 N. Goswami, A. Giri, S. Kar, M. S. Bootharaju, R. John, P. L. Xavier, T. Pradeep and S. K. Pal, *Small*, 2012, **8**, 3175–3184.

